PCCP

PAPER

View Article Online
View Journal | View Issue

Cite this: *Phys. Chem. Chem. Phys.*, 2024, **26**, 23168

On the composition and isomerism effect in the thermal and structural properties of choline chloride/hydroxyphenol deep eutectic solvents†

Paolo Casu, [a] Matteo Busato, *[a] Matteo Palluzzi, [a] Riccardo Spezia [b] and Paola D'Angelo *[a]

We have carried out a comparative study on three sets of eutectic mixtures based on choline chloride (ChCl) and hydroxyphenol isomers having two hydroxyl groups in the *ortho*-, *meta*-, and *para*-positions of the aromatic ring, namely catechol (Cate), resorcinol (Reso), and hydroquinone (Hydro), respectively. Differential scanning calorimetry highlighted a different thermal behavior of the mixtures depending on the composition and precursor isomerism. These systems behave as deep eutectic solvents (DESs) with the exception of the ChCl/Cate mixture at a 1 : 0.75 molar ratio, the ChCl/Reso mixtures at 1 : 2 and 1 : 3 molar ratios, and the ChCl/Hydro mixture at a 1 : 3 molar ratio. Infrared spectroscopy measurements and molecular dynamics simulations show that the stronger hydrogen-bonding (H-bonding) in the mixed states compared to the pure precursors is key for the formation of a DES. This interaction is mostly reliant on interconnected chloride anion coordination shells thanks to the two hydroxyl groups of the hydroxyphenol molecules, which can bridge between different anions to form an extended H-bond network. This structural arrangement maximizes the interactions and is enhanced by the 1 : 0.75 and 1 : 1 molar ratios, while increasing the hydroxyphenol concentration translates into a lowering of the total number of H-bonds formed in the mixture. This is the basis for the different thermal behavior and points to nearly equimolar compositions between the components, as ideally suited to achieve a DES from these precursors. The obtained insights are able to explain the structure–property relationships for the studied systems and are deemed useful for more conscious development of these inherently tuneable solvents.

Received 17th April 2024,
Accepted 29th July 2024

DOI: 10.1039/d4cp01575d

rsc.li/pccp

1 Introduction

Deep eutectic solvents (DESs) are a particular class of novel green media that excel as an alternative to traditional solvents to meet the safety and sustainability standards driving the ecological transition. Since their first appearance in 2003,[1] this class of solvents has been compared to that of ionic liquids (ILs) because of similarities like chemical and thermal stability, non-flammability, and negligible vapor pressure, in addition to high conductivity and low toxicity.[2,3] These qualities allow the use of DESs in different application fields such as electrochemistry, catalysis, synthesis, and extraction procedures of target compounds, among many others.[3–10]

Differently from ILs, DESs are formed from two or more parent compounds and exhibit, as a crucial feature, a melting point (MP) that is significantly underexpressed compared to the predicted one assuming thermodynamic ideality for the solid–liquid equilibrium (SLE) between the precursors.[11,12] Although this can occur for various molar ratios among the components, particular attention is usually devoted to compositions able to produce a liquid phase at operating conditions, *i.e.*, room temperature. For this reason, a rule of thumb to conceive a DES is the achievement of a liquid from solid starting materials, even if this is a feature in common with many ideal eutectics and not a strict definition of DESs.

Being constituted by two parent compounds, DESs possess several advantages over ILs and pure substances. For instance, their synthesis is a simple mixing of the starting compounds, usually under mild conditions like stirring and gentle heating, with no need for purification. In addition, their chemical-physical properties, *e.g.*, their MP, can be easily modulated by carefully choosing the precursors and their relative composition, so that DESs are often designated as "designer solvents".[2,13]

[a] *Dipartimento di Chimica, Sapienza Università di Roma, P.le A. Moro 5, 00185 Rome, Italy. E-mail: matteo.busato@uniroma1.it, p.dangelo@uniroma1.it*
[b] *Sorbonne Université, CNRS, Laboratoire de Chimie Théorique, 4 place Jussieu, 75005 Paris, France*

† Electronic supplementary information (ESI) available. See DOI: https://doi.org/10.1039/d4cp01575d

This unusual thermal behavior is deemed to be reliant upon the stronger intermolecular interactions between the mixed components relative to those established in their pure state. The nature of such interactions often consists of hydrogen bonding (H-bonding) and a practical way to classify the precursors is dividing them into H-bond donor (HBD) and H-bond acceptor (HBA) species, even if entropic factors and interactions of other natures have been found to concur with the MP depression.[14–18] However, the complexity of the interplay between the various components in the liquid phase often makes the nature of such interactions elusive and their quantification an intricate task.[15] For this reason, besides the constantly growing body of scientific literature dedicated to the synthesis of new DESs and their applications,[3,10] new knowledge could significantly benefit from a more thoughtful characterization of their chemical-physical properties, which could help to achieve a clearer structure–property relationship and drive a more conscious development of these inherently tunable media.

In the present article, we report a study on three different sets of mixtures formed by choline chloride (ChCl) and hydroxyphenol isomers presenting two hydroxyl groups in the *ortho*-, *meta*-, and *para*-positions to each other, namely 1,2-dihydroxybenzene also known as catechol (Cate), 1,3-dihydroxybenzene or resorcinol (Reso), and 1,4-dihydroxybenzene or hydroquinone (Hydro), respectively. The molecular structures of these compounds are depicted in Fig. 1. ChCl is one of the most widespread HBAs since Abbott and co-workers' pioneering paper about the prototypical DES "reline" (ChCl and urea in a 1 : 2 molar ratio)[1] due to its cheapness and bio-compatibility.[19] The hydroxyphenol family is particularly intriguing since it offers the possibility of investigating the role of the –OH position in the phenol ring and how eventually this can alter the H-bond network connecting the two species forming the eutectic mixtures.

In recent years, some experimental studies have been dedicated to defined sets of phenol-based DESs,[20,21] with a recent study[22] focusing on the chemical-physical characterization of DESs with some of the HBDs presented in this work, but limited to the ChCl/HBD 1 : 3 molar ratio. Here, we expand this investigation to ChCl/HBD (HBD = Cate, Reso, Hydro) mixtures at 1 : 0.75, 1 : 1, 1 : 2, and 1 : 3 molar ratios to elucidate the effect of composition on the thermal and structural properties of these systems. To this end, we used a combination of different techniques including differential scanning calorimetry (DSC), attenuated total reflection Fourier transform infrared (ATR-FTIR) spectroscopy, and classical molecular dynamics (MD) simulations. DSC measurements were used for thermal characterization of the mixtures, ATR-FTIR allowed the H-bonding analysis through the inspection of the O–H stretching (ν_{OH}) vibration, while the MD technique has been widely employed as a workhorse for the retrieval of atomistic interpretations of the molecular association in complex systems like DESs.[23–26] This combined approach has allowed us to elucidate the influence of the different components and their molar ratio on the liquid phase of these systems, with the aim of adding new knowledge to drive the development of these tunable media for application purposes.

2 Materials and methods

2.1 Chemicals and sample preparation

ChCl, Cate, Reso, and Hydro were purchased from Merck (Milan, Italy), with a stated purity of ≥99%. All compounds were dried under vacuum overnight at 338 K, then ChCl/Cate, ChCl/Reso, and ChCl/Hydro mixtures at 1 : 0.75, 1 : 1, 1 : 2, and 1 : 3 molar ratios were prepared by mixing the proper amount of the starting components in glass test tubes in an Ar-filled glovebox (<5 ppm H_2O). The samples were then stirred and heated at 363 K until homogeneous transparent liquids were obtained. ChCl/Reso and ChCl/Hydro mixtures appeared as colorless liquids, while ChCl/Cate formed brownish blends. All compositions provided a liquid phase except for the ChCl/Hydro 1 : 3 mixture.

2.2 DSC measurements

DSC thermograms were collected on the ChCl/Cate, ChCl/Reso, and ChCl/Hydro mixtures at various molar ratios of the components using a DSC821 instrument (Mettler-Toledo, Columbus, USA). A sample amount of about 5 mg was weighed and then sealed in a 40 μL aluminum pan. Samples were cooled from room temperature to 173 K with a −5 K min^{-1} rate, followed by a heating ramp to 373 K at 5 K min^{-1}. During all

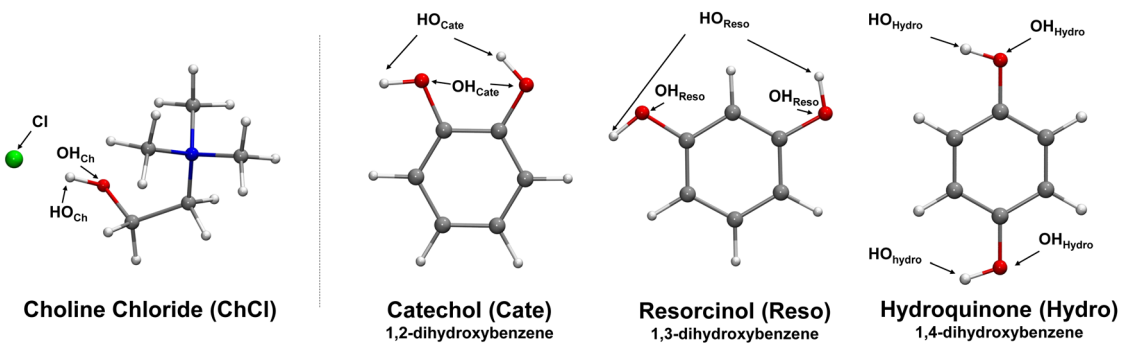

Fig. 1 Molecular structures of the ChCl, Cate, Reso, and Hydro precursors with the employed atom nomenclature (white, hydrogen; gray, carbon; red, oxygen; blue, nitrogen; green, chloride).

measurements, the furnace was purged with dry nitrogen with a 80 mL min^{-1} flow rate.

2.3 ATR-FTIR spectroscopy measurements

Infrared (IR) spectra were collected in ATR mode with a Bruker ALPHA spectrometer (ThermoFisher, Waltham, USA) equipped with a diamond crystal. The spectra of the ChCl/Cate, ChCl/Reso, and ChCl/Hydro mixtures were acquired in the liquid form. To this end, the samples were previously heated at about 343 K, then a drop was withdrawn and straightaway deposited to avoid crystallization on the ATR crystal. In this way, the samples were observed to persist in the supercooled liquid state long enough for data collection. Data were acquired on crystalline ChCl, Cate, Reso, and Hydro due to their higher MPs.[27] Absorbance spectra at room temperature were collected by co-adding 240 scans in the 4000–400 cm^{-1} spectral range with a 4 cm^{-1} resolution. The overall acquisition time took about four minutes. Spectral evolution was not observed during the measurement and thus water uptake from air moisture has been considered negligible.

2.4 Computational details

Classical MD simulations have been performed on the ChCl/Cate, ChCl/Reso, and ChCl/Hydro systems at 1 : 0.75, 1 : 1, 1 : 2, and 1 : 3 molar ratios. The all-atom optimized potentials for liquid simulations (OPLS-AA) force field [28] was used for all the species, except for the cholinium cation and chloride anion, which were described with the OPLS-compatible parameters by Canongia Lopes and Pádua.[29,30] van der Waals interactions were included *via* a Lennard-Jones potential with mixed terms constructed with the Lorentz–Berthelot combining rules, while the electrostatic interaction was represented by a Coulomb potential. An additional intramolecular Lennard-Jones potential was included to account for repulsion and dispersion between the vicinal hydroxyl groups in the Cate molecule, with parameters taken from Prampolini *et al.*[31] Periodic boundary conditions in all directions were applied to model the liquid state. A cut-off radius of 12.0 Å was employed for all non-bonded interactions, while the particle mesh Ewald method was used to account for the long-range electrostatic effects.[32,33]

To simulate the systems at 338 K, which is above the experimentally determined MP for all mixtures (*vide infra*), initial boxes were built with a number of atoms and box dimensions to reproduce the experimental density of the ChCl/Reso 1 : 0.75 mixture at 298 K, which is the only mixture with a MP below room temperature. These systems were then employed for density estimation with a 10 ns NPT run at 338 K and 1 atm. The computed densities were used to build the final cubic boxes of about 50 Å side length, with initial positions of the molecular species set randomly with the PACKMOL package.[34] Full details about the number of molecules and box dimensions are given in Table S1 of the ESI.† After energy minimization, these systems were equilibrated under NVT conditions through a heating ramp up to 500 K, remaining at this temperature for 12 ns, and then gradually cooled down to 338 K. High-temperature equilibrations were previously observed to be mandatory to speed up the dynamics of viscous liquids like DESs and ILs.[35–38] Production runs for data collection were carried out for 50 ns under NVT conditions. The Nosé–Hoover thermostat with a relaxation constant of 0.5 ps was employed for temperature control, while the Parrinello–Rahman barostat with a 1.0 ps coupling constant was employed in the case of the NPT simulations. The equations of motions were integrated using a leap-frog algorithm with a 1 fs time step, with trajectories saved every 100 steps. Constrictions for stretching vibrations involving hydrogen atoms were applied through the LINCS algorithm.[39] Simulations were performed with the 2020.2 version of the GROMACS package.[40] Trajectories visualization and data analysis were performed with the VMD 1.9.3 software.[41]

Quantum-chemical calculations were carried out on isolated (gas-phase) rotamers of the Cate molecule at the density functional theory (DFT) level. Geometry optimizations have been performed from initial configurations involving either an intramolecular H-bond between the two hydroxyl groups (Cate intra) or not (Cate inter). The B3LYP functional[42,43] was employed together with the 6-311++G(d,p) basis set and D3 Grimme's empirical dispersion corrections.[44] Vibrational analysis was carried out to confirm the absence of imaginary frequencies and that the stationary points were global minima. The IR spectrum was then reported without a scaling factor and using a Lorentzian function with a FWHM of 20 cm^{-1} to mimic the spectral width. Calculations were performed with the Gaussian 16 software.[45]

3 Results and discussion

3.1 Thermal characterization

As a starting point it is interesting to describe the different behaviour of the systems obtained by mixing ChCl with the three hydroxyphenol isomers at 1 : 0.75, 1 : 1, 1 : 2, and 1 : 3 molar ratios. The ChCl/Cate and ChCl/Reso mixtures formed a homogeneous liquid phase after gentle heating (363 K) at all the explored compositions. The ChCl/Hydro system, on the other hand, formed liquid mixtures for all molar ratios with the exception of the 1 : 3 composition, which remained solid even under more serious heating conditions.

Key information about the thermal behavior of these mixtures can be obtained from the DSC traces recorded for all the explored compositions apart from the ChCl/Hydro 1 : 3 mixture, as shown in Fig. 2. The temperature of the most important transitions, *i.e.*, the liquid–glass transition (T_g), cold crystallization (T_{cc}), and melting (T_m) are listed in Table S2 (ESI†). As concerns the ChCl/Cate system, the 1 : 1 and 1 : 3 mixtures display similar features, as a liquid–glass transition is detected at 193 K for the former composition and at 211 K for the latter one. Upon heating the glass, cold crystallization occurs at 256 K and 253 K, respectively, while further heating of these crystalline phases allows both the two mixtures to fully melt at T_m = 318 K. On the other hand, the ChCl/Cate 1 : 0.75 mixture evidences only one exothermic peak at 264 K resembling a crystallization. Finally, the ChCl/Cate 1 : 2 mixture does not

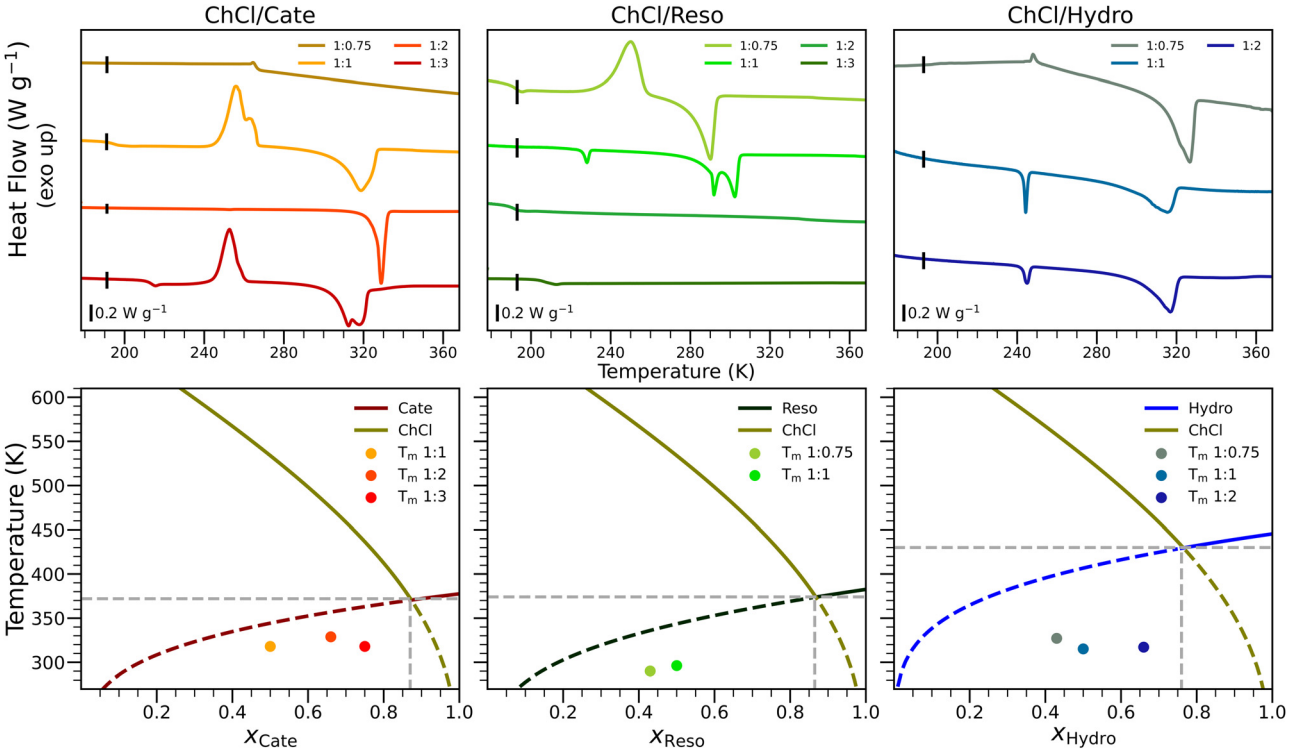

Fig. 2 Upper panels: DSC heating traces of the ChCl/Cate (left), ChCl/Reso (middle), and ChCl/Hydro (right) mixtures at different molar ratios of the components. A vertical black dashed line is present in each thermogram as a reference for the vertical axes. Lower panels: DSC-derived T_m values compared with the ideal phase diagram for the SLE equilibrium of the ChCl/Cate (left), ChCl/Reso (middle), and ChCl/Hydro (right) binary mixtures.

show any transition in the heating stage, apart from a melting process at T_m = 328 K.

The DSC thermogram recorded for the ChCl/Reso 1 : 0.75 mixture closely resembles those obtained for ChCl/Cate 1 : 1 and 1 : 3, as it shows three transition temperatures corresponding to T_g = 195 K, T_{cc} = 250 K, and T_m = 290 K. These three systems therefore evidenced a similar thermal behavior, which can be associated with their viscosity, since glass transition and cold crystallization are processes typical of polymers.[46] Conversely, the ChCl/Reso 1 : 1 mixture exhibits a melting temperature of 302 K. At the same time, the ChCl/Reso 1 : 2 and 1 : 3 thermograms show the presence of only two small flexes indicating a glass transition at low temperatures of 192 K and 213 K, respectively.

The DSC traces for the ChCl/Hydro mixtures show transitions at about 250 K, corresponding to an exothermic peak for the 1 : 0.75 system and endothermic peaks for the 1 : 1 and 1 : 2 ones. These contributions reveal a trickier thermal behavior that is difficult to understand due to the lack of information in the literature and the complex nature of these viscous systems. It is noteworthy that the endothermic peaks at 326 K (1 : 0.75), 315 K (1 : 1), and 316 K (1 : 2), correspond to the full melting of the mixtures.

Besides the inspection of the DSC traces, the analysis of the SLE between the precursors is imperative to characterize the eutectic behavior of these systems and to understand if the formation of a DES occurs. Such insight can be gained from the comparison between the experimental T_m value as obtained from the DSC measurements and the predicted one assuming thermodynamic ideality for the SLE phase diagram ($T_{m,ideal}$). DSC analysis enhanced eight T_m values for the ChCl/Cate 1 : 1, 1 : 2, and 1 : 3, ChCl/Reso 1 : 0.75 and 1 : 1, ChCl/Hydro 1 : 0.75, 1 : 1, and 1 : 2 systems (Table S2, ESI†). In the lower panels of Fig. 2 these temperatures are compared with the ideal SLE phase diagrams built from the enthalpies of fusion and melting temperatures of the pure ChCl[27] and hydroxyphenol[47] components. The ΔT values marking the difference between T_m and $T_{m,ideal}$ for the same composition are listed in Table S2 (ESI†). The experimental T_m values stand considerably below the ideal phase diagram (Fig. 2) so that the obtained ΔT values are negative (Table S2, ESI†). This evidence supports a DES thermal behavior for the compositions presenting a melting process.

3.2 ATR-FTIR results

Since H-bonding between the components is key to understanding the deviation from thermodynamic ideality in a DES, insights about this interaction have been obtained through ATR-FTIR spectroscopy measurements. To this end, ATR-FTIR spectra were recorded for the ChCl/Cate, ChCl/Reso, and ChCl/Hydro mixture compositions providing a liquid phase, and on the solid precursors.

In Fig. 3 we report the ATR-FTIR data in the spectral region corresponding to the ν_{OH} absorption band, which is known to be a useful mark for the H-bonding strength,[48] while the

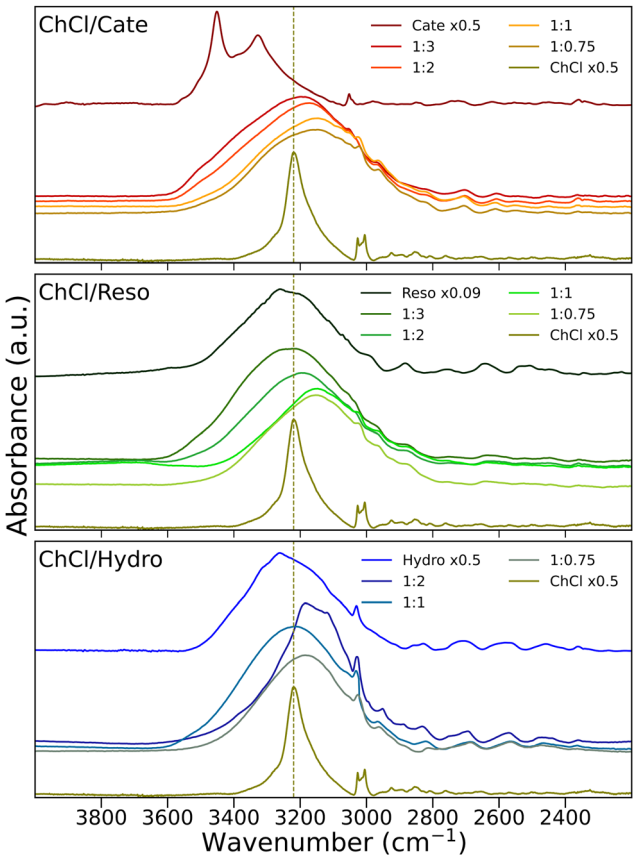

Fig. 3 Magnified ν_{OH} region of the ATR-FTIR spectra collected on the ChCl/Cate (top panel), ChCl/Reso (middle panel), and ChCl/Hydro (lower panel) mixtures at different molar ratios of the components and on the pristine starting compounds. A vertical dashed line corresponding to the maximum of the ν_{OH} absorption for the ChCl compound is reported as a guide to the eye.

complete spectra are shown in Fig. S1 (ESI†). The spectrum of solid ChCl shows a sharp and red-shifted peak that is compatible with the strongly H-bonded crystalline form of this compound. On the other hand, pristine Cate shows a more blue-shifted contribution split into two peaks (top panel of Fig. 3). Since this molecule carries two hydroxyl groups in the *ortho*-position to each other, in principle it is capable of both intra- and intermolecular H-bonding. As a consequence, the ν_{OH} contribution at lower frequency is tentatively associated with the stronger intramolecular H-bond, while the more blue-shifted one with the intermolecular interaction between different Cate molecules. To confirm this hypothesis, vibrational frequencies have been computed from DFT calculations carried out on two rotamers of the Cate molecule, *i.e.*, with either the hydroxyl hydrogen atoms pointing far away from each other, or with the hydrogen atom of one hydroxyl group pointing towards the oxygen atom of the other one (Fig. S2, ESI†). The simulated IR spectra show only one contribution in the ν_{OH} region for the former case, while this band is split into two peaks for the latter, confirming the assignment of the two ν_{OH} spectral components (Fig. 3). Conversely, the ν_{OH} absorption of pristine Reso and Hydro (middle and lower panel of Fig. 3, respectively) gives rise to broader bands, since these molecules are not capable of intramolecular H-bonding. Looking at the spectra collected for the ChCl/Cate, ChCl/Reso, and ChCl/Hydro mixtures, the interesting outcome is the red-shifted position of the ν_{OH} absorption, which is found even at lower frequencies for both the ChCl and HBD components for some compositions. This evidence supports a scenario where the H-bond interactions in the mixed states can be stronger than in the precursor compounds, even if compared to crystalline ChCl. Such an instance can reasonably be the basis of the ChCl/Cate, ChCl/Reso, and ChCl/Hydro DESs' formation for the analyzed molar ratios.

Focusing on the single sets, clear trends can be observed in the shift of the ν_{OH} band as a function of composition. In particular, while the ν_{OH} contributions for the 1 : 0.75 and 1 : 1 molar ratios of ChCl/Cate and ChCl/Reso are almost superimposable, a blue-shift is observed passing to the 1 : 2 and 1 : 3 compositions. Note that this trend is less clear for the ChCl/Hydro system, as the ν_{OH} band of the 1 : 2 mixture appears narrower since the contact with the ATR diamond crystal inevitably caused sample crystallization. Nevertheless, the whole result subtends for stronger H-bonding between the components when mixed at the 1 : 0.75 and 1 : 1 molar ratios, while this interaction weakens for higher concentrations of the HBD. Elucidating the nature of such interactions to find a rationale for these trends will be the subject of the following discussion.

3.3 MD simulations

From MD simulations it is possible to obtain atomistic information on the liquid states of the three systems as a function of the ChCl/HBD ratio. Note that we also simulated the ChCl/Hydro system at the 1 : 3 ratio, even if it was not possible to experimentally obtain it as a liquid phase. However, it is still noteworthy to compare simulation results obtained for this composition to understand how some properties change as a function of the molar ratio between the components. Since the ATR-FTIR analysis gave insights into the importance of H-bonding in the formation of these DESs, we focused in particular on this aspect.

First, we considered the radial distribution functions, $g(r)$, between selected atom pairs from the MD trajectories. The $g(r)$ values have been multiplied by the number density of the observed atoms (ρ) to avoid artifacts derived from the different compositions.[35,49] Since in ChCl-based DESs most of the H-bonding interactions involve the chloride anion,[23,50] a key $g(r)$ will be the one between this species and the hydrogen atom of the hydroxyl groups, of both the hydroxyphenol HBDs (HO_{HBD}) and the cholinium cation (HO_{Ch}). The distributions calculated for the Cl–HO_{HBD} and Cl–HO_{Ch} pairs are shown in Fig. 4, while the corresponding structural parameters are listed in Table 1. A first look delivers a feature common to all the $g(r)$ results, that is the presence of a well-defined peak with a maximum at about 2 Å (Table 1), followed by a depletion zone where the function goes to zero (Fig. 4). This shape and position of the peak maxima are compatible with the

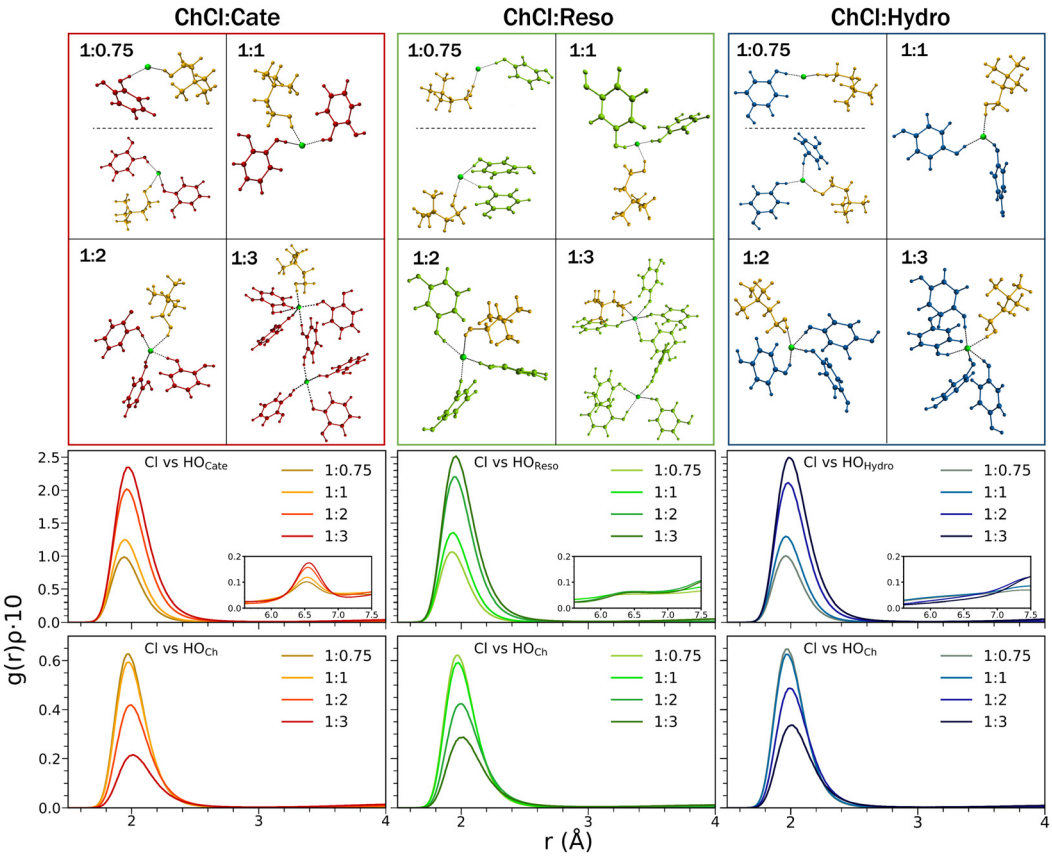

Fig. 4 Upper panels: Representative MD snapshots showing the coordination of the chloride anion in the various systems (red, Cate; green, Reso; blue, Hydro; yellow, cholinium cation; green, chloride anion). Lower panels: Radial distribution functions multiplied by the number density of the observed species, $g(r)\rho$, for the Cl–HO_{HBD} (HBD = Cate, Reso, Hydro) and Cl–HO_{Ch} pairs calculated from the MD simulations of the ChCl/Cate (left), ChCl/Reso (middle), and ChCl/Hydro (right) mixtures at different molar ratios of the components. The atom names are employed according to the nomenclature reported in Fig. 1.

Table 1 Structural parameters of the Cl–HO_{HBD} and Cl–HO_{Ch} $g(r)$ functions calculated from the MD simulations of the ChCl/Cate, ChCl/Reso, and ChCl/Hydro mixtures at different molar ratios of the components. R_{max} is the maximum position of the first peak and N is the coordination number calculated by integrating the $g(r)$ functions up to the cut-off distance of 3 Å. The atom names are employed according to the nomenclature reported in Fig. 1

		Cl–HO_{HBD}		Cl–HO_{Ch}	
		R_{max} (Å)	N	R_{max} (Å)	N
ChCl/Cate	1 : 0.75	1.94	1.4	1.97	1.0
	1 : 1	1.94	1.9	1.98	0.9
	1 : 2	1.96	3.3	1.99	0.7
	1 : 3	1.98	4.1	2.01	0.4
ChCl/Reso	1 : 0.75	1.93	1.5	1.97	1.0
	1 : 1	1.95	2.0	1.98	1.0
	1 : 2	1.95	3.5	2.00	0.8
	1 : 3	1.96	4.2	2.02	0.6
ChCl/Hydro	1 : 0.75	1.96	1.5	1.98	1.0
	1 : 1	1.96	1.9	1.97	1.0
	1 : 2	1.98	3.5	1.99	0.8
	1 : 3	1.99	4.3	2.01	0.6

establishment of strong H-bonds between the components,[25,26] as suggested by the ATR-FTIR data (Fig. 3). Note that the insets reported for the Cl–HO_{HBD} distributions highlight a small bump at about 6.5 Å for ChCl/Cate (Fig. 4). This is caused by the vicinal position of the two hydroxyl groups on the aromatic ring and suggests that the Cate molecule binds two different chloride anions with each hydroxyl group, rather than assuming a bidentate configuration binding one chloride with the hydrogen atoms of the two hydroxyl groups. This possibility is almost absent for the other two systems due to the longer distances between the hydroxyl groups in the Reso and Hydro molecules.

Considering single systems at different compositions, clear trends can be observed in the computed $g(r)$ results. In particular, the intensity of the Cl–HO_{HBD} distribution is found to increase with increasing HBD content, while the Cl–HO_{Ch} one decreases (Fig. 4). Note that the Cl–HO_{HBD} $g(r)$ functions have been multiplied by the number density of the HBD hydroxyl hydrogen atoms, therefore the growth in intensity of these functions is affected by the increase in the HBD concentration. This is not the case for the Cl–HO_{Ch} $g(r)$ functions because in all the systems the molar ratio between the chloride anion and the cholinium cation is the same (1 : 1). The decreasing trend of the Cl–HO_{Ch} $g(r)$ intensity suggests a less favorable H-bond interaction upon increasing the ChCl/HBD molar ratio. To gain

additional insights, we calculated the coordination numbers N by integrating the $g(r)$ functions up to the distance corresponding to the first minimum after the maximum, which typically defines a coordination shell. Concerning the Cl–HO_{HBD} distribution, taking into account that each HBD molecule can coordinate chloride anions with two hydroxyl groups, the maximum coordination number possible for this distribution is 1.5 for the 1 : 0.75 mixtures. On the other hand, for the same reason, a maximum N value of 2.0 can be obtained for the 1 : 1 molar ratio. The MD-calculated coordination numbers for the different HBD compositions are reported in Table 1. Here, one may note that a N value of 1.4–1.5 is obtained for the 1 : 0.75 molar ratio for all the investigated systems, while N stands in the 1.9–2.0 range for the 1 : 1 composition (Table 1). These values are very close to the expected ones, meaning that, among the HBD molecules present in solution, almost all can coordinate chloride anions with both the hydroxyl groups. However, a different situation is obtained for higher HBD concentrations. In particular, for the 1 : 2 ratio, each chloride anion can potentially be coordinated by 4.0 HBD hydroxyls, and this number is raised to 6.0 for the 1 : 3 ratio. The obtained coordination numbers are instead 3.3–3.5 for the 1 : 2 ratio and 4.1–4.4 for 1 : 3, thus lower than the expected values. This suggests that, among all the hydroxyl groups capable of H-bonding the chloride anion, a considerable amount is not involved in this interaction.

As far as the Cl–HO_{Ch} distribution is concerned, this interaction is deemed as one of the most important in ChCl-based DESs, since the one-to-one interplay between the chloride anion and the cholinium hydroxyl group present in the crystal structure of ChCl is substantially retained even after the eutectic formation.[23,25,35,50,51] Indeed, a N value of 1.0–0.9 is obtained for the 1 : 0.75 and 1 : 1 molar ratios in all the three systems (Table 1). This value is found to decrease for increasing HBD compositions, down to 0.4–0.6 for the 1 : 3 molar ratio. This also shows that the H-bond between the chloride anion and the cholinium cation is affected by the mixture composition and that the ChCl/HBD 1 : 0.75 and 1 : 1 ratios are ideally suited to maximize this interaction.

We have then calculated the number of H-bonds between the chloride anion and the hydroxyl groups of the HBD and cholinium cation components during the MD trajectory, which is listed in Table S4 (ESI†). To compare the different compositions, we have divided these values by the number of chloride anions in each system, thus obtaining the average number of H-bonds per chloride anion. The results are plotted in Fig. 5 as a function of the mixture composition. In the case of the Cl–HO_{HBD} interaction, a red dashed line indicates the maximum number of H-bonds that each chloride anion can establish with the HBD counterpart, *i.e.*, 1.5, 2.0, 4.0, and 6.0 for the 1 : 0.75, 1 : 1, 1 : 2, and 1 : 3 molar ratios, respectively. Note that this value corresponds to 1.0 for the Cl–HO_{Ch} interaction, independently from the composition, as previously stated. Similarly to what was obtained from the analysis of the $g(r)$ functions, the average number of H-bonds per chloride anion almost matches the maximum one for both interactions in the case of the 1 : 0.75 and 1 : 1 compositions. Differently,

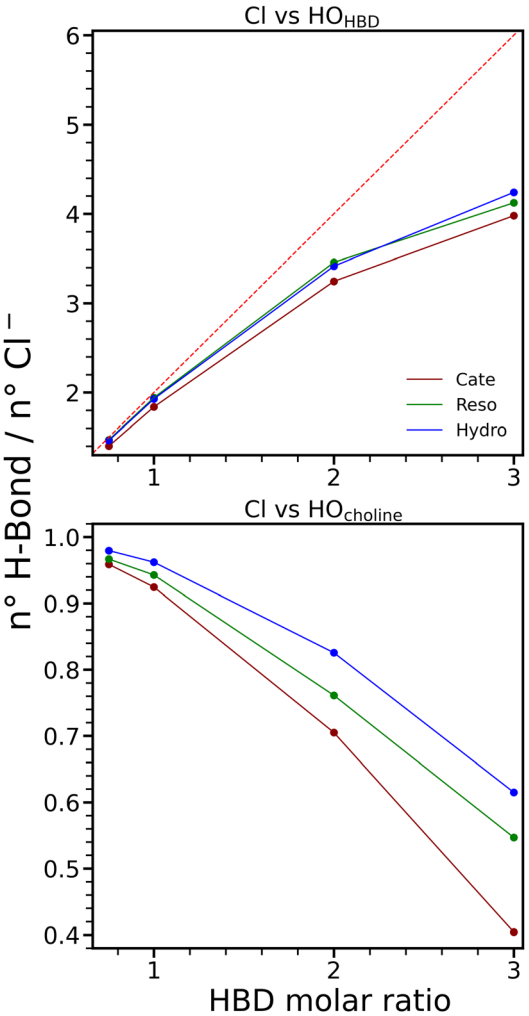

Fig. 5 Average number of H-bonds per chloride anion with the hydroxyl hydrogen atom of the HBD (top panel) and cholinium cation (lower panel) as a function of the HBD molar ratio calculated from the MD simulations of the ChCl/Cate, ChCl/Reso, and ChCl/Hydro mixtures at different molar ratios of the components. The red dashed line in the top panel represents the maximum number of H-bonds possible per chloride anion at each composition.

this number drops down from the expected value when increasing the HBD ratio. This result confirms that the H-bonding with the chloride anion is maximized for ChCl/HBD molar ratios up to 1 : 1, while higher HBD concentrations are not optimal for fully exploiting this interaction.

The overall structural picture therefore suggests the establishment of interconnected chloride anion coordination spheres thanks to the mediation of the HBD components. This arrangement can be monitored from the Cl–Cl $g(r)$ functions shown in Fig. S3 (ESI†). Here, an intense contribution at about 6 Å can be observed for the 1 : 0.75 and 1 : 1 molar ratios, which is significantly lowered for higher HBD contents. The snapshots in the upper panels of Fig. 4 are representative of this picture: for the 1 : 0.75 and 1 : 1 molar ratio each chloride anion interacts with the hydroxyl groups of two different HBD molecules and one cholinium cation. The HBD component can

bridge between two different anions thanks to the two hydroxyl functionalities to form Cl–HBD–Cl chains. Increasing the HBD concentration produces a less favorable optimization of these interactions due to the saturation of the chloride anion coordination sphere and consequent steric exclusion. Note that the cholinium cation, besides H-bonding through the hydroxyl group, can simultaneously interact with the chloride anion, with the cationic core centered on the nitrogen atom. This interaction has been previously found to occur through the tripodal $CH_3\cdots Cl$ structure in other ChCl-based DESs[25,35,51] and could reasonably complete the chloride anion coordination sphere to further promote the bridging between different coordination spheres.

Finally, the hydroxyl groups not interacting with the chloride anion could be involved in cholinium–HBD, HBD–HBD, and cholinium–cholinium interactions, as supported by the $g(r)$ functions reported in Fig. S4–S7 (ESI†). All these distributions display a well-defined peak with a maximum at about 2 Å, which is compatible with an H-bond interaction. While the intensity of these distributions is low and comparable for the 1 : 0.75 and 1 : 1 molar ratios, it increases for higher HBD contents, showing that the excess hydroxyphenol molecules, displaced from the chloride anion coordination sphere, interact with each other and with other cholinium cations.

4 Conclusions

In this work, we have characterized three different sets of eutectic mixtures formed by ChCl with hydroxyphenol isomers carrying two hydroxyl groups in the *ortho*-, *meta*-, and *para*-positions to each other. The parent compounds were mixed at different molar ratios to elucidate the effect of mixture composition and precursor isomerism on the thermal and structural properties.

According to the thermal analysis carried out by DSC measurements, the synthesized systems can be classified as DESs, since their experimental MPs are underexpressed compared to the predicted one from the ideal SLE phase diagram, with the exception of the ChCl/Cate mixture at 1 : 0.75 molar ratio, and the ChCl/Reso 1 : 2 and 1 : 3 mixtures, which show no melting points in the DSC traces, while the ChCl/Hydro 1 : 3 mixture does not form a liquid phase.

Inspection of the ν_{OH} band by ATR-FTIR measurements shows that H-bonding in the liquid phases can be stronger than in the pure precursors, this being the driving force for the DESs' achievement. The H-bond association is higher for the 1 : 0.75 and 1 : 1 molar ratios, while this interaction weakens for higher contents of the hydroxyphenol component.

MD simulations allowed us to find a rationale for these trends and to elucidate the possible interactions contributing to DES formation. The structural arrangement sees both cholinium cations and hydroxyphenol molecules acting as H-bond donors towards the chloride anion. The hydroxyphenol component can bridge between different chloride anion coordination shells to form an extended H-bond network owing to the two hydroxyl groups. This structural arrangement maximizes the interactions and is best promoted by the 1 : 0.75 and 1 : 1 molar ratios, while increasing the hydroxyphenol concentration lowers the total number of H-bonds due to steric exclusion around the saturated chloride anion coordination spheres. This situation promotes the H-bonding among cholinium cations and hydroxyphenol molecules, which is initially negligible and less effective in stabilizing the liquid phase.

The inspection of the H-bonding association by our combined experimental and theoretical outcome provided a rationale for the different thermal behavior and strongly suggests that compositions around the equimolar one between the precursors are ideal to achieve a DES for the studied systems. The considerations reported here are useful as reference knowledge for a more conscious synthesis and handling of these "designer solvents" for multipurpose applications.

Data availability

The data supporting this article have been included as part of the ESI.†

Conflicts of interest

There are no conflicts to declare.

Acknowledgements

The authors acknowledge the European Union-Next-GenerationEU under the Italian Ministry of University and Research (MUR), Network 4 Energy Sustainable Transition – NEST project – CUP B53C22004070006 and the Italian Ministry of University and Research (MUR) for the PRIN project "MOF-MTM: tailoring Metal–Organic Frameworks for the direct Methane To Methanol conversion under mild conditions" number 2022SFC459. PhD program on green topics of the PON Research and Innovation 2014–2020 'Education and research for recovery – REACT-EU' is acknowledged.

Notes and references

1 A. P. Abbott, G. Capper, D. L. Davies, R. K. Rasheed and V. Tambyrajah, *Chem. Commun.*, 2003, 70–71.
2 M. Francisco, A. van den Bruinhorst and M. C. Kroon, *Angew. Chem., Int. Ed.*, 2013, **52**, 3074–3085.
3 E. L. Smith, A. P. Abbott and K. S. Ryder, *Chem. Rev.*, 2014, **114**, 11060–11082.
4 Q. Zhang, K. D. O. Vigier, S. Royer and F. Jérôme, *Chem. Soc. Rev.*, 2012, **41**, 7108–7146.
5 Y. Dai, G.-J. Witkamp, R. Verpoorte and Y. H. Choi, *Anal. Chem.*, 2013, **85**, 6272–6278.
6 P. Liu, J.-W. Hao, L.-P. Mo and Z.-H. Zhang, *RSC Adv.*, 2015, **5**, 48675–48704.
7 J. Huang, X. Guo, T. Xu, L. Fan, X. Zhou and S. Wu, *J. Chromatogr. A*, 2019, **1598**, 1–19.

8 A. K. Dwamena, *Separations*, 2019, **6**, 9.
9 A. P. Abbott, *Curr. Opin. Green Sustainable Chem.*, 2022, **36**, 100649.
10 B. B. Hansen, S. Spittle, B. Chen, D. Poe, Y. Zhang, J. M. Klein, A. Horton, L. Adhikari, T. Zelovich and B. W. Doherty, *et al.*, *Chem. Rev.*, 2021, **121**, 1232–1285.
11 M. A. Martins, S. P. Pinho and J. A. Coutinho, *J. Solution Chem.*, 2019, **48**, 962–982.
12 D. O. Abranches and J. A. Coutinho, *Curr. Opin. Green Sustainable Chem.*, 2022, **35**, 100612.
13 R. Hayes, G. G. Warr and R. Atkin, *Chem. Rev.*, 2015, **115**, 6357–6426.
14 A. van den Bruinhorst, C. Corsini, G. Depraetère, N. Cam, A. A. H. Pádua and M. Costa Gomes, *Faraday Discuss.*, 2024, DOI: **10.1039/D4FD00048J**.
15 M. Busato, G. Mannucci, L. A. Rocchi, M. E. Di Pietro, A. Capocefalo, E. Zorzi, P. Casu, D. Veclani, F. Castiglione, A. Mele, A. Martinelli, P. Postorino and P. D'Angelo, *ACS Sustainable Chem. Eng.*, 2023, **11**, 8988–8999.
16 M. Busato, G. Mannucci, V. Di Lisio, A. Martinelli, A. Del Giudice, A. Tofoni, C. Dal Bosco, V. Migliorati, A. Gentili and P. D'Angelo, *ACS Sustainable Chem. Eng.*, 2022, **10**, 6337–6345.
17 A. J. Peloquin, J. M. McCollum, C. D. McMillen and W. T. Pennington, *Angew. Chem., Int. Ed.*, 2021, **60**, 22983–22989.
18 D. O. Abranches, N. Schaeffer, L. P. Silva, M. A. R. Martins, S. P. Pinho and J. A. P. Coutinho, *Molecules*, 2019, **24**, 3687.
19 K. Radošević, M. Cvjetko Bubalo, V. Gaurina Srček, D. Grgas, T. Landeka Dragičević and I. Radojčić Redovniković, *Ecotoxicol. Environ. Saf.*, 2015, **112**, 46–53.
20 W. Guo, Y. Hou, S. Ren, S. Tian and W. Wu, *J. Chem. Eng. Data*, 2013, **58**, 866–872.
21 J. Zhu, K. Yu, Y. Zhu, R. Zhu, F. Ye, N. Song and Y. Xu, *J. Mol. Liq.*, 2017, **232**, 182–187.
22 F. Cappelluti, A. Mariani, M. Bonomo, A. Damin, L. Bencivenni, S. Passerini, M. Carbone and L. Gontrani, *J. Mol. Liq.*, 2022, **367**, 120443.
23 M. E. Di Pietro, O. Hammond, A. van den Bruinhorst, A. Mannu, A. A. H. Pádua, A. Mele and M. Costa Gomes, *Phys. Chem. Chem. Phys.*, 2021, **23**, 107–111.
24 A. Triolo, F. Lo Celso and O. Russina, *J. Mol. Liq.*, 2023, **372**, 121151.
25 M. Busato, V. Migliorati, A. Del Giudice, V. Di Lisio, P. Tomai, A. Gentili and P. D'Angelo, *Phys. Chem. Chem. Phys.*, 2021, **23**, 11746–11754.
26 M. Busato, A. Del Giudice, V. Di Lisio, P. Tomai, V. Migliorati, A. Gentili, A. Martinelli and P. D'Angelo, *ACS Sustainable Chem. Eng.*, 2021, **9**, 12252–12261.
27 A. van den Bruinhorst, J. Avila, M. Rosenthal, A. Pellegrino, M. Burghammer and M. Costa Gomes, *Nat. Commun.*, 2023, **14**, 6684.
28 W. L. Jorgensen, D. S. Maxwell and J. Tirado-Rives, *J. Am. Chem. Soc.*, 1996, **118**, 11225–11236.
29 J. N. Canongia Lopes and A. A. H. Pádua, *J. Phys. Chem. B*, 2004, **108**, 16893–16898.
30 J. N. Canongia Lopes and A. A. H. Pádua, *J. Phys. Chem. B*, 2006, **110**, 19586–19592.
31 G. Prampolini, M. Campetella and A. Ferretti, *Phys. Chem. Chem. Phys.*, 2023, **25**, 2523–2536.
32 T. Darden, D. York and L. Pedersen, *J. Chem. Phys.*, 1993, **98**, 10089–10092.
33 U. Essmann, L. Perera, M. L. Berkowitz, T. Darden, H. Lee and L. G. Pedersen, *J. Chem. Phys.*, 1995, **103**, 8577–8593.
34 L. Martínez, R. Andrade, E. G. Birgin and J. M. Martínez, *J. Comput. Chem.*, 2009, **30**, 2157–2164.
35 V. Migliorati, F. Sessa and P. D'Angelo, *Chem. Phys. Lett.*, 2019, **737**, 100001.
36 M. Busato, A. Tofoni, G. Mannucci, F. Tavani, A. Del Giudice, A. Colella, M. Giustini and P. D'Angelo, *Inorg. Chem.*, 2022, **61**, 8843–8853.
37 M. Busato, P. D'Angelo and A. Melchior, *Phys. Chem. Chem. Phys.*, 2019, **21**, 6958–6969.
38 M. Busato, P. D'Angelo, A. Lapi, M. Tolazzi and A. Melchior, *J. Mol. Liq.*, 2020, **299**, 112120.
39 B. Hess, H. Bekker, H. J. Berendsen and J. G. Fraaije, *J. Comput. Chem.*, 1997, **18**, 1463–1472.
40 M. J. Abraham, T. Murtola, R. Schulz, S. Páll, J. C. Smith, B. Hess and E. Lindahl, *SoftwareX*, 2015, **1–2**, 19–25.
41 W. Humphrey, A. Dalke and K. Schulten, *J. Mol. Graphics*, 1996, **14**, 33–38.
42 A. D. Becke, *J. Chem. Phys.*, 1993, **98**, 5648–5652.
43 C. Lee, W. Yang and R. G. Parr, *Phys. Rev. B*, 1988, **37**, 785–789.
44 S. Grimme, J. Antony, S. Ehrlich and H. Krieg, *J. Chem. Phys.*, 2010, **132**, 154104.
45 M. J. Frisch, G. W. Trucks, H. B. Schlegel, G. E. Scuseria, M. A. Robb, J. R. Cheeseman, G. Scalmani, V. Barone, G. A. Petersson, H. Nakatsuji, X. Li, M. Caricato, A. V. Marenich, J. Bloino, B. G. Janesko, R. Gomperts, B. Mennucci, H. P. Hratchian, J. V. Ortiz, A. F. Izmaylov, J. L. Sonnenberg, D. Williams-Young, F. Ding, F. Lipparini, F. Egidi, J. Goings, B. Peng, A. Petrone, T. Henderson, D. Ranasinghe, V. G. Zakrzewski, J. Gao, N. Rega, G. Zheng, W. Liang, M. Hada, M. Ehara, K. Toyota, R. Fukuda, J. Hasegawa, M. Ishida, T. Nakajima, Y. Honda, O. Kitao, H. Nakai, T. Vreven, K. Throssell, J. A. Montgomery, Jr., J. E. Peralta, F. Ogliaro, M. J. Bearpark, J. J. Heyd, E. N. Brothers, K. N. Kudin, V. N. Staroverov, T. A. Keith, R. Kobayashi, J. Normand, K. Raghavachari, A. P. Rendell, J. C. Burant, S. S. Iyengar, J. Tomasi, M. Cossi, J. M. Millam, M. Klene, C. Adamo, R. Cammi, J. W. Ochterski, R. L. Martin, K. Morokuma, O. Farkas, J. B. Foresman and D. J. Fox, *Gaussian16 Revision C.01*, Gaussian Inc., Wallingford, CT, 2016.
46 M. Jaffe and J. D. Menczel, *Thermal analysis of textiles and fibers*, Woodhead Publishing, 2020.
47 S. P. Verevkin and S. A. Kozlova, *Thermochim. Acta*, 2008, **471**, 33–42.
48 D. Ojha, K. Karhan and T. Kühne, *Sci. Rep.*, 2018, **8**, 16888.
49 V. Migliorati, A. Gibiino, A. Lapi, M. Busato and P. D'Angelo, *Inorg. Chem.*, 2021, **60**, 10674–10685.
50 V. Migliorati and P. D'Angelo, *Chem. Phys. Lett.*, 2021, **777**, 138702.
51 O. S. Hammond, D. T. Bowron and K. J. Edler, *Green Chem.*, 2016, **18**, 2736–2744.

